Preprints of the 21st IFAC World Congress (Virtual)
Berlin, Germany, July 12-17, 2020

Robust Adaptive Control of a Multirotor with an Unknown Suspended Payload

A.P. Erasmus * **H.W. Jordaan** **

* *Electrical and Electronic Engineering Department, Stellenbosch University, South Africa (email: 18177654@sun.ac.za)*
** *Electrical and Electronic Engineering Department, Stellenbosch University, South Africa (email: wjordaan@sun.ac.za)*

Abstract:
This paper addresses the problem of a multirotor carrying an unknown suspended payload, allowed to swing in one axis. The payload is unknown in the sense that its parameters, such as the payload mass and cable length, are unknown and its state, the swing angles, are not available for measurement. The suspended payload alters the flight dynamics of the vehicle considerably and the flight controllers need to minimize this effect.
A robust model reference adaptive control technique is designed and implemented to minimize the effect of the suspended payload on the vehicle while allowing the controller to adapt to account for the unknown payload. The controller is modified to reject external disturbances and to be robust in the presence of sensor noise and drift. In simulation, this technique proves to dampen the oscillations caused by the payload.
A quadrotor was built to practically demonstrate the effectiveness of the controller. The PX4 flight control stack is considered for the firmware of the vehicle. The model reference adaptive controller was implemented and succeeded to dampen the oscillations caused by the payload in a practical flight.

Keywords: Learning and adaptation in autonomous vehicles, Multirotor, UAV, Suspended payload, Model reference adaptive control, Robust.

1. INTRODUCTION

The use of multirotors, known as rotary-wing Unmanned Aerial Vehicles (UAVs), for tasks that involve transport offers several advantages over conventional ground transport systems. These advantages include travel to hard-to-reach locations, shorter travel distances and avoiding traffic. The applications include consumer deliveries, military transport, medical and emergency needs, and search and rescue.

Consumer deliveries with UAVs are becoming quite attractive with companies such as Flirtey [Mack, 2017], Alphabet [Hern, 2019] and Amazon [Hern, 2016] investigating the potential of the market. The use of multirotors for transportation regarding medical needs are also gaining attraction [Zraick, 2019].

These projects involve a grasped payload rigidly attached to the body of the vehicle. This approach restricts the shape and size of the payload. Suspended payloads can be used to overcome this limitation.

Suspended payloads are attached to the multirotor through a rope, cable or rigid rod. These payloads are free to swing underneath the multirotor and significantly alters the flight characteristics of the vehicle. Suspended payloads dominate the literature because of the advantages they have over grasped payloads and the difficulty of the problem. Researchers consider both known and unknown suspended payloads, outlined in Fig. 1.

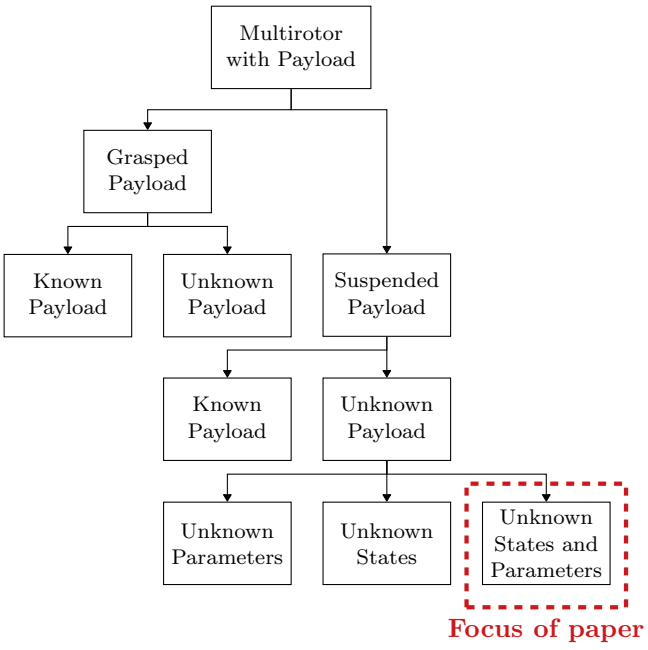

Fig. 1. Summary of literature study on multirotors with payloads.

There are mainly two types of approaches to minimize the effect of the payload on the multirotor:

- Minimum swing trajectory generation
- Anti-swing controllers

Minimum swing trajectory generation uses a trajectory that inherently does not cause large payload oscillations. These methods usually make use of an open-loop design using dynamic programming [Palunko et al., 2012b] or input shaping [Sadr et al., 2014], but are not robust against parameter uncertainties or external disturbances.

Anti-swing controllers are designed to actively damp the oscillations caused by the payload. These methods are all based on feedback control, using the payload angle as the feedback term. Alothman et al. [2015] designed a Linear Quadratic Regulator (LQR) controller and Goodarzi et al. [2015] proposes a geometric control technique. Other research groups propose hybrid controllers consisting of two parts, one part handling the multirotor position and another handling the payload angles [Yang and Xian, 2018, Raffo and De Almeida, 2016].

It is clear that various control techniques can be used to stabilize the multirotor and payload system given the payload's parameters and/or state. When considering an unknown payload, one needs to estimate the payload mass and cable length to adapt the controller accordingly. Dai et al. [2014] implemented an adaptive algorithm to compensate for an unknown payload mass and Yang and Xian [2019] implemented an adaptive controller to compensate for an unknown cable length. These algorithms assume that the payload's state is known.

In reality, one also needs to measure or estimate the payload's state. Bisgaard et al. [2010] used a downward-facing camera on a helicopter to estimate the cable length and swing angles to control the vehicle and payload system with minimum swing. De Angelis [2019] used the available onboard sensors and knowledge of the payload's parameters to estimate the state of the payload and control the system accordingly. Palunko et al. [2012a] designed an adaptive controller to estimate the center of mass (CoM) of a multirotor with a known payload and adapt the controller based on these estimates. Guerrero-Sánchez et al. [2017] designed a controller that is independent of the payload's state using Interconnection and Damping Assignment-Passivity Based Control, based on known payload parameters.

This paper addresses the problem of stabilizing a multirotor with an unknown suspended payload, of which its state is not available for measurement. Fig. 1 summarizes the different problems found in literature regarding this topic and highlights the focus of this paper. A payload with only 1 Degree of Freedom (DoF), meaning that it is restricted to swing in one axis, is considered. By using the principle of superposition, the proposed solution can be duplicated in the other axis to allow control of a payload capable of swinging in both axes.

A robust adaptive controller, based on the Model Reference Adaptive Control (MRAC) architecture, is designed to minimize the effect of the payload on the vehicle and ensure stable flight. The controller is independent of predetermined knowledge and real-time measurements of the state of the suspended payload. A quadrotor vehicle is used to demonstrate the effectiveness of the solution in a practical experiment.

This paper is outlined as follows: Section 2 derives the mathematical model of the quadrotor and suspended payload system, Section 3 describes the design of the MRAC scheme for the quadrotor, Section 4 introduces the hardware used for the practical flight, Section 5 showcases and discusses the practical flight results and Section 6 draws some conclusions.

2. MODELLING

Consider the quadrotor and coordinate frames shown in Fig. 2. The North East Down (NED) inertial frame is indicated by $\mathcal{I} = \{\bar{\boldsymbol{x}}_\mathcal{I}, \bar{\boldsymbol{y}}_\mathcal{I}, \bar{\boldsymbol{z}}_\mathcal{I}\}$ and the body frame of the quadrotor is indicated by $\mathcal{B} = \{\bar{\boldsymbol{x}}_\mathcal{B}, \bar{\boldsymbol{y}}_\mathcal{B}, \bar{\boldsymbol{z}}_\mathcal{B}\}$.

The quadrotor has six degrees of freedom which are described by the kinetic equations (1) and (2).

$$\boldsymbol{F}_\mathcal{B} = m_q \dot{\boldsymbol{V}}_\mathcal{B} + \boldsymbol{\Omega}_\mathcal{B} \times m_q \boldsymbol{V}_\mathcal{B}, \tag{1}$$

$$\boldsymbol{M}_\mathcal{B} = \boldsymbol{I}_q \dot{\boldsymbol{\Omega}}_\mathcal{B} + \boldsymbol{\Omega}_\mathcal{B} \times \boldsymbol{I}_q \boldsymbol{\Omega}_\mathcal{B}, \tag{2}$$

where $\boldsymbol{F}_\mathcal{B}$ and $\boldsymbol{M}_\mathcal{B}$ are the body forces and moments acting in on the vehicle. The parameters, m_q and $\boldsymbol{I}_q$ denote the mass and mass moment of inertia, respectively, of the quadrotor, and $\boldsymbol{V}_\mathcal{B}$ and $\boldsymbol{\Omega}_\mathcal{B}$ denote the body linear velocity and the body angular velocity. The quadrotor kinematic equations are given by

$$\begin{bmatrix} \dot{q}_0 \\ \dot{q}_1 \\ \dot{q}_2 \\ \dot{q}_3 \end{bmatrix} = \frac{1}{2} \begin{bmatrix} q_0 & -q_1 & -q_2 & -q_3 \\ q_1 & q_0 & -q_3 & q_2 \\ q_2 & q_3 & q_0 & -q_1 \\ q_3 & -q_2 & q_1 & q_0 \end{bmatrix} \begin{bmatrix} 0 \\ \Omega_{\mathcal{B}_X} \\ \Omega_{\mathcal{B}_Y} \\ \Omega_{\mathcal{B}_Z} \end{bmatrix} \text{ and} \tag{3}$$

$$\dot{\boldsymbol{X}}_\mathcal{I} = \boldsymbol{R}_V^{-1} \boldsymbol{V}_\mathcal{B}, \tag{4}$$

where $\bar{\boldsymbol{q}} = [q_0, q_1, q_2, q_3]^T$ is a unit quaternion with q_0 being the magnitude, $\boldsymbol{X}_\mathcal{I} = [X_{\mathcal{I}_X}, X_{\mathcal{I}_Y}, X_{\mathcal{I}_Z}]^T$ is the position of the quadrotor in the inertial frame and

$$\boldsymbol{R}_V = \begin{bmatrix} q_0^2 + q_1^2 + q_2^2 + q_3^2 & 2(q_1 q_2 + q_0 q_3) & 2(q_1 q_3 - q_0 q_2) \\ 2(q_1 q_2 - q_0 q_3) & q_0^2 - q_1^2 + q_2^2 - q_3^2 & 2(q_2 q_3 + q_0 q_1) \\ 2(q_1 q_3 + q_0 q_2) & 2(q_2 q_3 - q_0 q_1) & q_0^2 - q_1^2 - q_2^2 + q_3^2 \end{bmatrix} \tag{5}$$

is the rotation matrix from the inertial frame to the body frame of the vehicle.

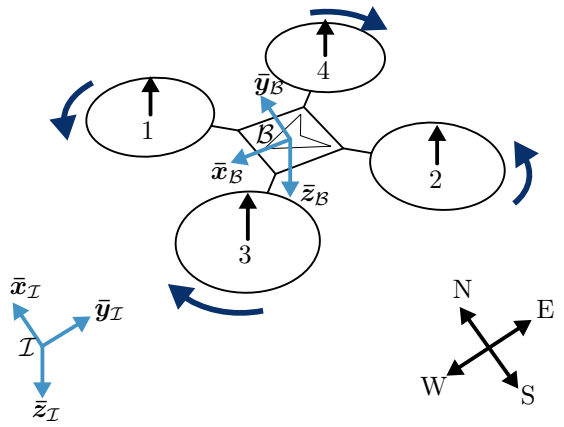

Fig. 2. Quadrotor and coordinate frames illustration.

The forces and moments acting in on the vehicle are

- the actuators,
- gravity,
- aerodynamic drag, and
- the suspended payload.

In this paper, only the forces and moments caused by the suspended payload are discussed in further detail. The dynamics of the suspended payload are derived using Lagrangian mechanics. Consider the quadrotor and payload model shown in Fig. 3. The following assumptions are made regarding the payload:

- the payload link is rigid and weightless,
- the payload is considered to be a point mass,
- the payload is attached to the CoM of the vehicle, and
- the payload angle β is restricted to $-\frac{\pi}{2} \leq \beta \leq \frac{\pi}{2}$.

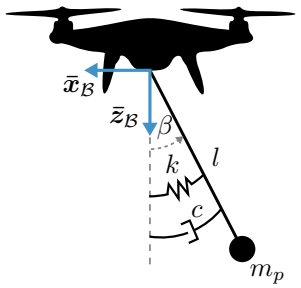

Fig. 3. Quadrotor with a suspended payload.

The Lagrangian is given by

$$\mathcal{L} = \frac{1}{2} m_q \left(\dot{x}_q^2 + \dot{z}_q^2\right) + \frac{1}{2} m_p \left(\dot{x}_p^2 + \dot{z}_p^2\right) + m_p g z_p, \tag{6}$$

where x_q and z_q are the horizontal and vertical positions of the quadrotor, respectively, x_p and z_p are the horizontal and vertical positions of the payload. The variables m_q and m_p are the mass of the quadrotor and payload, and g is the gravitational acceleration constant. The Euler Lagrange equation is given as

$$\frac{d}{dt}\left(\frac{\partial \mathcal{L}}{\partial \dot{\boldsymbol{p}}}\right) - \frac{\partial \mathcal{L}}{\partial \boldsymbol{p}} = \begin{bmatrix} 0 \\ 0 \\ -k\beta - c\dot{\beta} \end{bmatrix}, \tag{7}$$

where $\boldsymbol{p} = [x_q, z_q, \beta]^T$. Solving the Euler Lagrange equation yields the differential equations

$$\ddot{x}_q = -\frac{(c\dot{\beta}+k\beta)(m_q+m_p)\cos\beta + l m_q m_p \sin\beta(l\dot{\beta}^2 + g\cos\beta)}{l m_q (m_q+m_p)} \tag{8}$$

$$\ddot{z}_q = -\frac{(c\dot{\beta}+k\beta)(m_q+m_p)\sin\beta - l m_q m_p \cos\beta(l\dot{\beta}^2 + g\cos\beta)}{l m_q (m_q+m_p)} \tag{9}$$

$$\ddot{\beta} = -\frac{(c\dot{\beta}+k\beta)(m_q+m_p) + g l m_q m_p \sin\beta}{l^2 m_q m_p} \tag{10}$$

where l is the rod length, k and c are the spring and damper coefficients, respectively, and β is the swing angle. The effect of aerodynamic drag on the payload is also modeled.

The force that the payload exerts on the quadrotor in the inertial frame can be calculated by

$$\boldsymbol{F}_{\mathcal{I}}^P = (m_q + m_p) \begin{bmatrix} \ddot{x}_q \\ 0 \\ \ddot{z}_q \end{bmatrix}. \tag{11}$$

Transforming this to the body frame, yields

$$\boldsymbol{F}_{\mathcal{B}}^P = \boldsymbol{R}_V \boldsymbol{F}_{\mathcal{I}}^P. \tag{12}$$

The derived differential equations are implemented to simulate the quadrotor and payload system. The simulated quadrotor is based on the practical quadrotor described in Section 4.

3. CONTROLLER DESIGN

The flight control system architecture is based on a cascaded control architecture consisting of linear Proportional Integral Derivative (PID) controllers, as shown in Fig. 4. The two outer loops control the quadrotor's inertial position and inertial linear velocity, respectively. A desired inertial force $\boldsymbol{F}_{\mathcal{I}}$ is commanded by the inertial linear velocity controller, which is converted to the desired attitude. The inner control loops act in the body frame and actuate the motors to achieve the desired attitude.

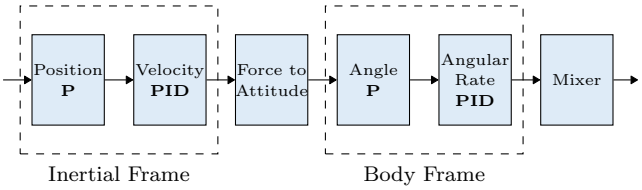

Fig. 4. Control system architecture.

The suspended payload only affects the translational component of the vehicle, because of the assumption that it is attached to the CoM of the vehicle. The effect of a 2 kg payload with a 1 m rod is seen in the inertial linear velocity, shown in Fig. 5, when a position step input is commanded. Therefore, the north linear velocity controller needs to be altered to dampen the oscillations caused by the unknown suspended payload.

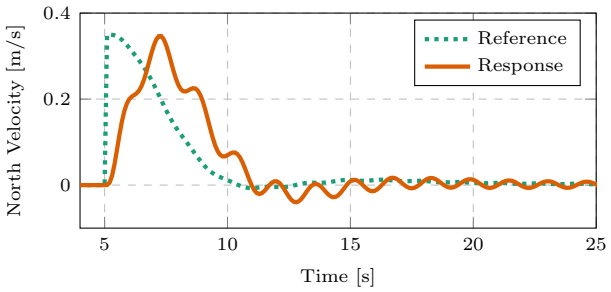

Fig. 5. The quadrotor's north velocity after a position step input.

An adaptive controller, based on the MRAC architecture [Ioannou and Sun, 2012], is designed for the north velocity controller as the controller needs to adapt to the specific payload attached.

3.1 Overview of MRAC

MRAC is an adaptive control scheme that changes the dynamics of the closed-loop system to that of a predetermined reference model. The MRAC structure is shown in Fig. 6.

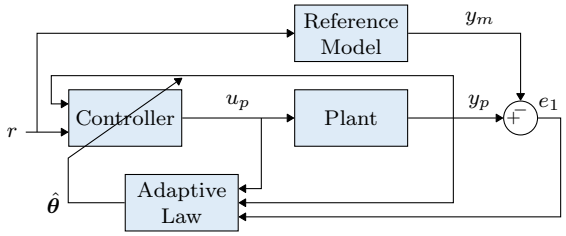

Fig. 6. Block diagram of the MRAC architecture.

The plant and reference model are described by

$$G_p(s) = k_p \frac{Z_p(s)}{R_p(s)}, \text{ and} \tag{13}$$

$$W_m(s) = k_m \frac{Z_m(s)}{R_m(s)}. \tag{14}$$

The MRAC scheme effectively performs pole-zero cancellation to transform the closed-loop response of the system to that of the reference model. It consists of a control law and an adaptive law. Direct MRAC is considered in this case, where the adaptive law produces estimates of the control parameters directly. This requires fewer computations than the indirect approach.

The control law and adaptive law are designed separately. The design processes of both laws are discussed next.

3.2 Control Law

The MRAC control law is given as

$$u_p = \boldsymbol{\theta}_1^T \frac{\boldsymbol{\alpha}(s)}{\Lambda(s)} u_p + \boldsymbol{\theta}_2^T \frac{\boldsymbol{\alpha}(s)}{\Lambda(s)} y_p + \theta_3 y_p + c_0 r, \tag{15}$$

where

$$\boldsymbol{\alpha}(s) = \begin{cases} \boldsymbol{\alpha}_{n-2}(s) = [s^{n-2}, \ldots, s, 1]^T, & \text{for } n \geq 2 \\ 0, & \text{for } n = 1 \end{cases} \tag{16}$$

$$\Lambda(s) = \Lambda_0(s) Z_m(s), \text{ and} \tag{17}$$

n is the order of the denominator of the plant $G_p(s)$. In the non-adaptive case, the controller parameter vector $\boldsymbol{\theta} = [\boldsymbol{\theta}_1^T,\ \boldsymbol{\theta}_2^T,\ \theta_3,\ c_0]^T$ is chosen so that the transfer function from r to y_p is $W_m(s)$. In the adaptive case, these parameters are replaced with their estimates $\hat{\boldsymbol{\theta}}$.

The linear plant of the north velocity of the quadrotor and payload system is derived as

$$\frac{V_{\mathcal{I}_X}(s)}{F_{\mathcal{I}_X}(s)} = \frac{1}{m_q} \frac{s^2 + \frac{c}{l^2 m_p} s + \frac{k}{l^2 m_p} + \frac{g}{l}}{s^3 + \frac{c(m_q+m_p)}{l^2 m_q m_p} s^2 + \left[\frac{k(m_q+m_p)}{l^2 m_q m_p} + \frac{g}{l}\frac{m_q+m_p}{m_q}\right] s}. \tag{18}$$

The goal is to dampen the oscillations caused by the payload. Therefore, a first-order reference model is chosen as it has no oscillations. The reference model is given as

$$W_m(s) = \omega_m \cdot \frac{1}{s + \omega_m}. \tag{19}$$

The term $\frac{\boldsymbol{\alpha}(s)}{\Lambda(s)}$ serves as a filter and is required for higher order systems to effectively perform pole-zero cancellation of the closed-loop system, in order to adapt it to the reference model. To achieve this, $\Lambda(s)$ is chosen as

$$\Lambda(s) = s^2 + 2\zeta_\lambda \omega_\lambda s + \omega_\lambda^2, \text{ and} \tag{20}$$

$$\boldsymbol{\alpha}(s) = [s,\ 1]^T. \tag{21}$$

The design variables of the MRAC control law are ω_m, ω_λ and ζ_λ. The bandwidth of the reference model ω_m is chosen according to the bandwidth of the quadrotor and its inner controllers. The filter parameters, ω_λ and ζ_λ, can be chosen a bit more arbitrarily.

The ideal control parameters $\boldsymbol{\theta}$, which results in a closed-loop system exactly equal to that of the reference model are derived as

$$\boldsymbol{\theta}_1 = \begin{bmatrix} \theta_{11} \\ \theta_{12} \end{bmatrix} = \begin{bmatrix} 2\zeta_\lambda \omega_\lambda - \frac{c}{l^2 m_p} \\ \omega_\lambda^2 - \frac{g}{l} - \frac{k}{l^2 m_p} \end{bmatrix}, \tag{22}$$

$$\boldsymbol{\theta}_2 = \begin{bmatrix} \theta_{21} \\ \theta_{22} \end{bmatrix} = \begin{bmatrix} m_q \omega_\lambda^2 \left(4\zeta_\lambda^2 - 1\right) + \frac{m_q+m_p}{l^2 m_p}\left(g l m_p + k - 2c\zeta_\lambda \omega_\lambda\right) \\ 2 m_q \omega_\lambda^3 \zeta_\lambda - \frac{c}{l^2 m_p}\left(m_q + m_p\right) \end{bmatrix}, \tag{23}$$

$$\theta_3 = -m_q \left(2\zeta_\lambda \omega_\lambda + \omega_m\right) + \frac{c\left(m_q + m_p\right)}{l^2 m_p}, \text{ and} \tag{24}$$

$$c_0 = m_q \omega_m. \tag{25}$$

These equations give insight on how to choose the initial values of the control parameters and the filter parameters ω_λ and ζ_λ. Notice that if ω_λ is chosen quite large, it will dominate the control parameters. Therefore, the effect of the payload becomes smaller and the control law becomes more robust against parameter uncertainty.

This effect is illustrated in Fig. 7, where the MRAC control law is applied to the linear plant for a 3 kg payload with a 1.5 m rod. The parameter ζ_λ is chosen as $\zeta_\lambda = 0.9$. The chosen values of the control parameters $\boldsymbol{\theta}$ assume no payload and are reduced to

$$\boldsymbol{\theta}_{1_0} = \begin{bmatrix} 2\zeta_\lambda \omega_\lambda \\ \omega_\lambda^2 \end{bmatrix}, \tag{26}$$

$$\boldsymbol{\theta}_{2_0} = \begin{bmatrix} m_q \omega_\lambda^2 \left(4\zeta_\lambda^2 - 1\right) \\ 2 m_q \omega_\lambda^3 \zeta_\lambda \end{bmatrix}, \tag{27}$$

$$\theta_{3_0} = -m_q \left(2\zeta_\lambda \omega_\lambda + \omega_m\right), \text{ and} \tag{28}$$

$$c_{0_0} = m_q \omega_m. \tag{29}$$

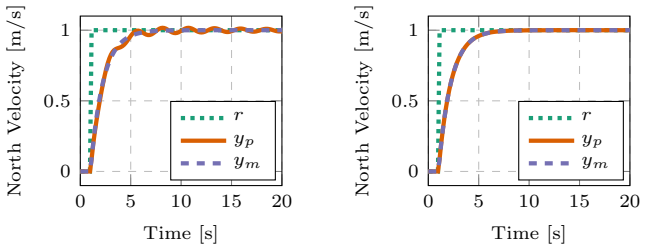

(a) $\omega_\lambda = 5$ (b) $\omega_\lambda = 50$

Fig. 7. The north velocity response of the linear plant with the MRAC control law.

It is clear that in the case of $\omega_\lambda = 50$ the response follows the reference model exactly, in contrast to the case of $\omega_\lambda = 5$ where the oscillations caused by the payload are still present. Practically, the parameter ω_λ is considered large if it falls outside of the bandwidth of the velocity dynamics of the vehicle.

Applying the control law to the non-linear model yields a response that does not sufficiently follow the reference model. This can be seen in the first step response of Fig. 8. Therefore an adaptive law is needed to account for the non-linearities of the system.

3.3 Adaptive Law

An adaptive law adapts the control parameters based on the error between the plant output and reference model output, given by $e_1 = y_p - y_m$. A normalized adaptive law is used as it is independent of the magnitude of the reference signal, r. The adaptive law is derived using the Strictly Positive Real (SPR)-Lyapunov design approach and is described by

$$\frac{d\hat{\boldsymbol{\theta}}}{dt} = -\boldsymbol{\Gamma}\epsilon\boldsymbol{\phi}\text{sgn}\left(\frac{k_p}{k_m}\right), \tag{30}$$

where

$$\epsilon = \frac{e_1 - \hat{e}_1}{1 + n_s^2}, \tag{31}$$

$$\hat{e}_1 = \rho(u_f - \hat{\boldsymbol{\theta}}^T\boldsymbol{\phi}), \tag{32}$$

$$\dot{\rho} = \gamma\epsilon(u_f - \hat{\boldsymbol{\theta}}^T\boldsymbol{\phi}), \tag{33}$$

$$n_s^2 = \boldsymbol{\phi}^T\boldsymbol{\phi} + u_f^2, \tag{34}$$

$$u_f = W_m(s)u_p, \text{ and} \tag{35}$$

$$\boldsymbol{\phi} = W_m(s)\boldsymbol{\omega}. \tag{36}$$

The variable $\boldsymbol{\Gamma}$ is a matrix with the respective adaptive gains on the diagonal, γ is the adaptive gain for the parameter ρ, $\text{sgn}(x)$ is the signum function, and

$$\boldsymbol{\omega} = \left[\frac{\boldsymbol{\alpha}(s)}{\Lambda(s)}u_p,\ \frac{\boldsymbol{\alpha}(s)}{\Lambda(s)}y_p,\ y_p,\ r\right]^T. \tag{37}$$

Given that ω_λ is large, it was decided to make the adaptive gains for the control parameters, $\boldsymbol{\theta}_1$ and $\boldsymbol{\theta}_2$, zero, resulting in no adaptation of those parameters. This decision is based on the fact that the payload has a negligible effect on those parameters given a large ω_λ. The parameters θ_3 and c_0 are allowed to adapt and appropriate adaptive gains are chosen. The MRAC response of a quadrotor with a 2 kg payload and 1 m rod length is shown in Figures 8 and 9.

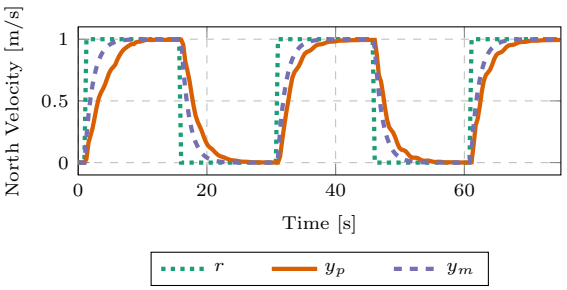

Fig. 8. The MRAC north velocity response of the non-linear quadrotor model.

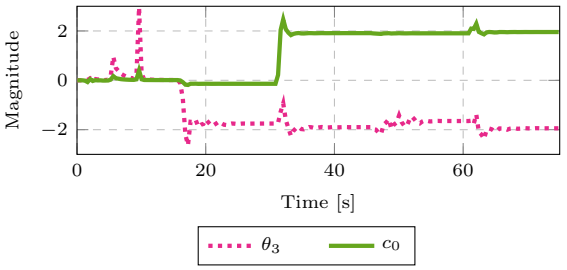

Fig. 9. The change in the adaptive parameters from their initial values.

The adaptive parameters settle around new values resulting in an improvement in the response. The robustness of the MRAC scheme is discussed next.

3.4 Robustness

Practical systems suffer from sensor noise, sensor drift, and external disturbances. These phenomena have severe effects on the MRAC scheme. This is illustrated in Fig. 10, where the system is under the influence of sensor noise, sensor drift, and a disturbance introduced at time $t = 40$ s.

The first problem to address is with regards to the adaptation. It is clear from Equation (30) that adaptation will take place as long as there is an error between the output and reference model signal. When the system is under the influence of sensor noise and sensor drift, an error will always exist. Therefore, MRAC runs the risk of always adapting its parameters which can lead to them diverging. This is prevented by the implementation of two techniques known as leakage (Ioannou and Sun [2012]) and parameter bounds. Leakage changes the adaptive law to

$$\frac{d\hat{\boldsymbol{\theta}}}{dt} = -\boldsymbol{\Gamma}\text{sgn}\left(\frac{k_p}{k_m}\right)\left[\epsilon\boldsymbol{\phi} + w\left(\hat{\boldsymbol{\theta}} - \boldsymbol{\theta}_0\right)\right], \tag{38}$$

where w is known as the leakage term. Leakage pushes the adaptive parameters back to their initial values, keeping them from diverging. Eventually, both the adaptive and leakage terms reach an equilibrium, stabilizing the adaptive parameters. The switching-σ technique is used as the choice for w. It only activates the leakage term when the adaptive parameters are outside some acceptable bounds.

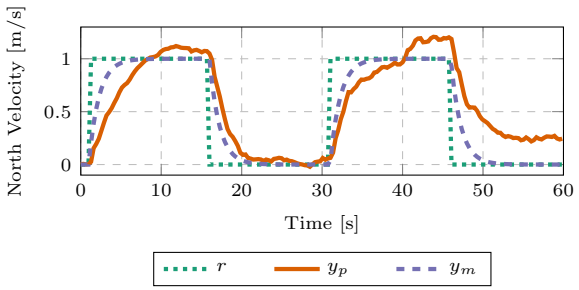

Fig. 10. The MRAC north velocity response with sensor noise and a disturbance at $t = 40$ s.

Leakage is sometimes referred to as a "soft-bound" as it does not put a limit on the parameters, but act in such a way to try and keep the parameters within some acceptable bounds. In this case, hard parameter bounds are also implemented to ensure that the parameters never exceed a certain upper and lower bound. This concludes the improvements made to the adaptive law to keep the adaptive parameters from diverging when dealing with practical sensors.

Practical systems suffer from external disturbances, which leads to non-zero steady-state tracking. The adaptive parameters will adapt, due to the existing error, but won't necessarily converge to a value capable of removing the steady-state error. Sun et al. [1994] explored performance improvements of MRAC which improves both the tran-

sient and steady-state response. The modification adds a term to the control law, resulting in

$$u_p = \hat{\boldsymbol{\theta}}_1^T \frac{\boldsymbol{\alpha}(s)}{\Lambda(s)} u_p + \hat{\boldsymbol{\theta}}_2^T \frac{\boldsymbol{\alpha}(s)}{\Lambda(s)} y_p + \hat{\theta}_3 y_p + \hat{c}_0 r + u_a, \text{ where} \quad (39)$$

$$u_a = -C(s)e_1, \text{ and} \quad (40)$$

$$C(s) = \frac{\hat{c}_0 W_m^{-1}(s)}{(\tau_c s + 1)^{n^*} - 1}. \quad (41)$$

The time-constant τ_c is a parameter to be designed and n^* is the difference in the orders of the denominator and numerator of the plant $G_p(s)$. The term u_a is proportional to the error between the plant and reference model, which results in transient improvements when the error is large and zero steady-state tracking performance when the error is small. The design parameter τ_c adjusts the aggressiveness of the term u_a. The parameter is chosen to be at least twice as fast as the reference model, which is deemed sufficiently fast to not affect the reference model. The results of the simulation in Fig. 10 with the added robustness improvements are shown in Fig. 11.

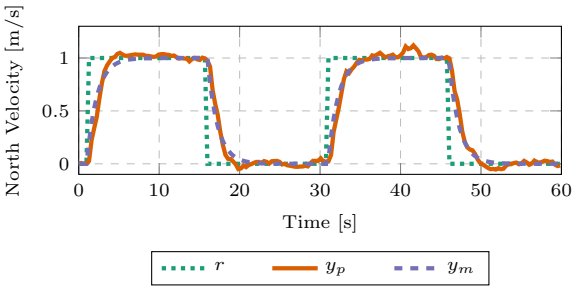

Fig. 11. The modified MRAC north velocity response with sensor noise and a disturbance at $t = 40$ s.

It is clear that both the transient and steady-state response have improved and the disturbance at time $t = 40$ s is sufficiently rejected. The error between the plant and reference model has reduced, but leakage and parameter bounds are implemented to prevent the adaptive parameters from diverging. This concludes the controller design of the quadrotor and suspended payload system.

4. HARDWARE AND SYSTEM OVERVIEW

The quadrotor and payload system shown in Fig. 12 was built to practically demonstrate the effectiveness of the MRAC scheme. The quadrotor consists of a 960 mm frame with a T-motor propulsion system and a total mass of 4.5 kg. A rod, allowed to swing only in one axis, is attached to the quadrotor with a potentiometer to measure the swing angle. The measured angle is logged for offline analysis purposes.

The onboard flight controller is a Pixhawk running the open-source flight control stack PX4. The controller gains were adjusted to the designed gains of the custom-built quadrotor and the linear velocity controller was replaced with the MRAC scheme. PX4 supports both Software-in-the-Loop (SIL) and Hardware-in-the-Loop (HIL) simulations using the Gazebo simulator. The simulation environment incorporates noise models of the sensors, simulating effects such as high-frequency noise, low-frequency drift, and sensor biases. Thus, this simulation environment is ideal to test the implemented algorithms under the influence of these effects.

Fig. 12. Custom-built quadrotor.

A model of the custom-built quadrotor and a 2 kg payload with a 1 m rod was implemented to test in the Gazebo environment. The results of such a simulation, given position step inputs, are shown in Fig. 13 and the adaptive parameters are shown in Fig. 14. In the simulation, MRAC was activated at $t = 45$ s to compare the response of the non-adaptive controller and the MRAC scheme.

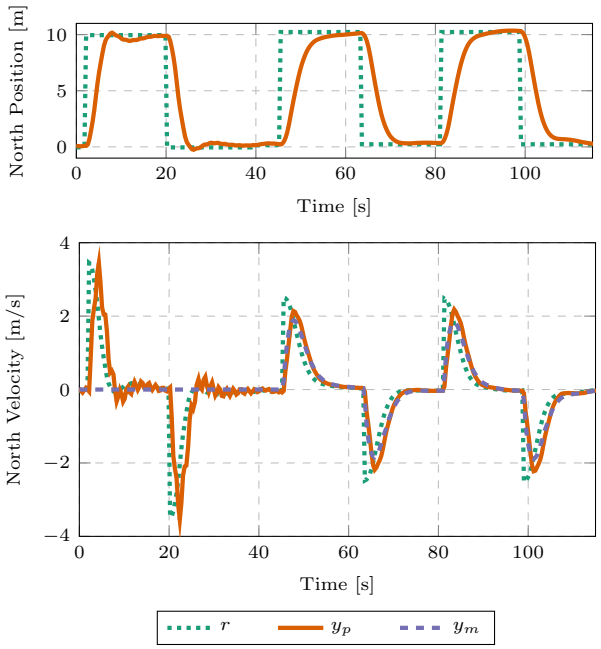

Fig. 13. Gazebo simulation results of north position steps.

The MRAC scheme sufficiently damps the oscillations caused by the unknown payload. It is difficult to see the adaptation in the response, given position step inputs, but the adaptive parameters indicate that adaptation takes place.

5. PRACTICAL RESULTS

A test flight is set up to demonstrate the effectiveness of the proposed MRAC scheme in a practical flight. The

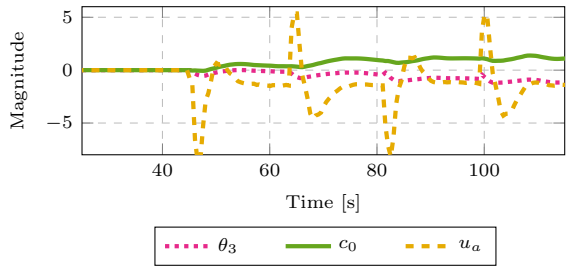

Fig. 14. The change in the adaptive parameters from their initial values.

following flights, each with a different payload, are considered:

- no payload,
- 1 kg payload with a 1 m rod, and a
- 2 kg payload with a 1 m rod.

The practical flight consisted of performing multiple 10 m position steps. Firstly, position step inputs were commanded with a standard PID controller activated. It is undesirable to induce large oscillations, such as those shown in Fig. 13, into the practical system as it can yield an unsafe flight. Therefore, the PID control gains are optimized for the specific payload of each flight, yielding fewer oscillations. Thereafter, the MRAC scheme is activated and the position steps are repeated.

The response of the tuned PID controller, shown in Fig. 15, is compared to the response of the MRAC scheme, shown in Fig. 16, for the flight with the 1 kg payload. The measured payload swing angle of the flight, for the respective cases, is shown in Fig. 17 and the adaptive parameters are shown in Fig. 18.

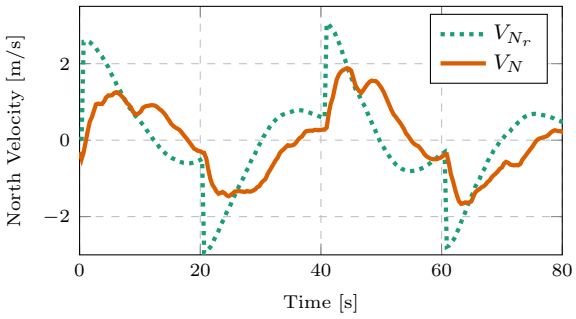

Fig. 15. The practical response of the tuned PID controller with a 1 kg payload.

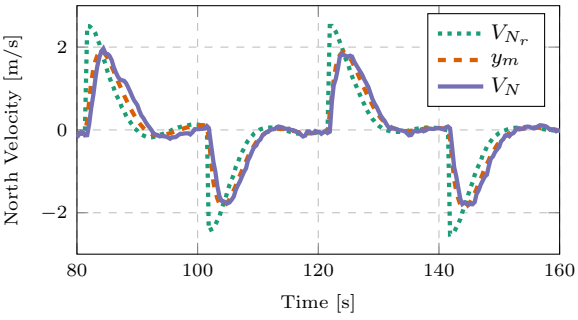

Fig. 16. The practical response of the MRAC scheme with a 1 kg payload.

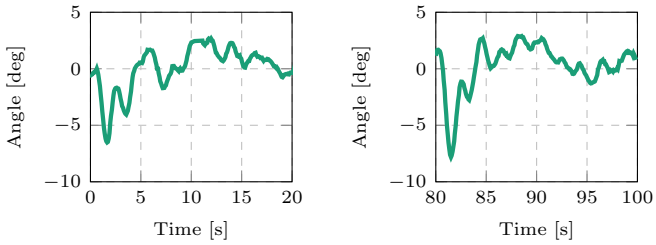

(a) PID response (b) MRAC response

Fig. 17. The measured payload angle of the practical flight with the 1 kg payload.

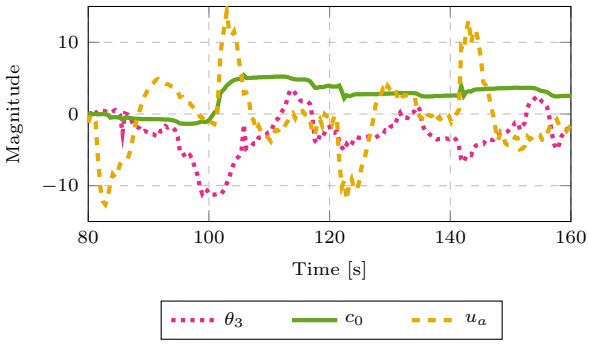

Fig. 18. The change in the adaptive parameters from their initial values of the practical flight with the 1 kg payload.

It is clear that both the tuned PID controller and the MRAC scheme are able to damp the oscillations caused by the payload, as the north velocity response contains no oscillations and the swing angle remains small. The adaptive parameters of the practical flight adapt more than that of the simulation results. This is due to the presence of larger sensor noise and drift, causing the adaptive controller to react more aggressively to be able to follow the reference model.

The MRAC scheme performs much better than the tuned PID case in terms of following the reference signal. The MRAC scheme provides consistent performance, regardless of the payload, as shown in Fig. 19, where the responses of all three flights are compared.

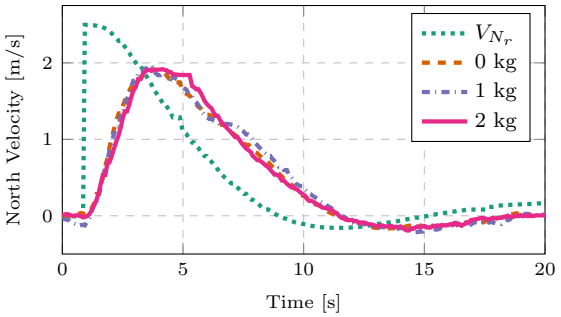

Fig. 19. Comparison of the practical response for different payloads.

It is concluded that the MRAC scheme for the unknown payload case can damp the payload oscillations just as well as the tuned PID case for a known payload, in a

practical flight. The MRAC scheme outperforms the tuned PID controller in terms of reference following, however, an analysis revealed that the MRAC scheme commands a more aggressive control signal which requires more control energy. This is a trade-off that is made with the MRAC scheme. However, the consistent performance that the MRAC scheme provides for different payloads is more desirable in this case.

6. CONCLUSION

In this paper, the problem of a quadrotor carrying an unknown suspended payload is considered. The suspended payload's parameters are unknown and its state is not available for measurement. The payload significantly affects the flight dynamics of the vehicle by inducing oscillations into the system. In this paper, the suspended payload is restricted to swing only in one axis. A MRAC scheme is proposed to damp these oscillations and can adapt to the specific payload attached.

The MRAC control law is made robust with the choice of design parameters and with the addition of a term that is proportional to the error of the output and the reference model. The MRAC adaptive law is only allowed to change the parameters of the control law that will result in a significant difference as the other parameters are made robust and will not change as much.

It was found in simulation that the MRAC scheme can sufficiently damp the oscillations caused by the payload while providing good tracking performance and disturbance rejection. The successful simulation results served as a motivation for a practical flight test.

A practical flight test was conducted with different payloads. The results illustrate that the MRAC scheme can effectively minimize the effect of the suspended payload on the quadrotor vehicle. The MRAC scheme produced consistent results for three different payloads, proving that it can adapt to the specific payload attached to the vehicle. The practical flight proves that MRAC is a viable solution for transporting different suspended payloads via an UAV.

Future work includes duplicating the proposed solution in the other axis to allow the stabilization of a multirotor with a suspended payload able to swing in both axes. In this case, the principle of superposition is applied to extend the problem to the case of a payload with 2 DoF.

REFERENCES

Alothman, Y., Jasim, W., and Gu, D. (2015). Quad-rotor lifting-transporting cable-suspended payloads control. *2015 21st International Conference on Automation and Computing: Automation, Computing and Manufacturing for New Economic Growth, ICAC 2015*.

Bisgaard, M., la Cour-Harbo, A., and Dimon Bendtsen, J. (2010). Adaptive control system for autonomous helicopter slung load operations. *Control Engineering Practice*, 18, 800–811.

Dai, S., Lee, T., and Bernstein, D.S. (2014). Adaptive control of a quadrotor UAV transporting a cable-suspended load with unknown mass. *Proceedings of the IEEE Conference on Decision and Control*, 2015-February, 6149–6154.

De Angelis, E.L. (2019). Swing angle estimation for multicopter slung load applications. *Aerospace Science and Technology*.

Goodarzi, F.A., Lee, D., and Lee, T. (2015). Geometric control of a quadrotor UAV transporting a payload connected via flexible cable. *International Journal of Control, Automation and Systems*.

Guerrero-Sánchez, M.E., Mercado-Ravell, D.A., Lozano, R., and García-Beltrán, C.D. (2017). Swing-attenuation for a quadrotor transporting a cable-suspended payload. *ISA Transactions*, 68, 433–449.

Hern, A. (2016). Amazon claims first successful prime air drone delivery. URL `https://www.theguardian.com/technology/2016/dec/14/amazon-claims-first-successful-prime-air-drone-delivery`. Accessed: 2019-05-20.

Hern, A. (2019). Customers in australian capital can get food and coffee delivered via drone. URL `https://techcrunch.com/2019/04/09/customers-in-australian-capital-can-get-food-and-coffee-delivered-via-drone/`. Accessed: 2019-05-20.

Ioannou, P. and Sun, J. (2012). *Robust Adaptive Control*. Dover Publications. URL `http://www.amazon.com/Robust-Adaptive-Control-Electrical-Engineering/dp/0486498174`.

Mack, B. (2017). Flirtey is making domino's pizza delivery by drone available for regular folks. URL `https://idealog.co.nz/tech/2017/06/flirtey-making-dominos-pizza-delivery-drone-available-regular-folks`. Accessed: 2019-05-20.

Palunko, I., Cruz, P., and Fierro, R. (2012a). Agile load transportation : Safe and efficient load manipulation with aerial robots. *IEEE Robotics and Automation Magazine*.

Palunko, I., Fierro, R., and Cruz, P. (2012b). Trajectory generation for swing-free maneuvers of a quadrotor with suspended payload: A dynamic programming approach. *Proceedings - IEEE International Conference on Robotics and Automation*.

Raffo, G.V. and De Almeida, M.M. (2016). Nonlinear robust control of a quadrotor UAV for load transportation with swing improvement. *Proceedings of the American Control Conference*.

Sadr, S., Moosavian, S.A.A., and Zarafshan, P. (2014). Dynamics modeling and control of a quadrotor with swing load. *Journal of Robotics*.

Sun, J., Olbrot, A., and Polis, M. (1994). Robust stabilization and robust performance using model reference control and modeling error compensation. *IEEE Transactions on Automatic Control*.

Yang, S. and Xian, B. (2018). Robust control design for the quadrotor UAV with a suspended payload. *Proceedings of 2018 IEEE 8th Annual International Conference*.

Yang, S. and Xian, B. (2019). Energy-based nonlinear adaptive control design for the quadrotor UAV system with a suspended payload. *IEEE Transactions on Industrial Electronics*.

Zraick, K. (2019). Like uber for organs: drone delivers kidney to maryland woman. URL `https://www.nytimes.com/2019/04/30/health/drone-delivers-kidney.html`. Accessed: 2019-05-20.